This is the pre-peer reviewed version of the article: Mohanty J R, Verma B B, Ray P K, Parhi D R K, Prediction of mode-I overload-induced fatigue crack growth rates using neuro-fuzzy approach, *Expert Systems with Applications,* **37**(2010), 3075-3087, which has been published in the final form at
http://www.sciencedirect.com/science/journal/09574174

Prediction of mode-I overload-induced fatigue crack growth rates using neuro-fuzzy approach

J. R. Mohanty[a*], B. B. Verma[a], P. K. Ray[b*], D. R. K Parhi[b]

[a] *Department of Metallurgical and Materials Engineering*

[b] *Department of Mechanical Engineering*

National Institute of Technology, Rourkela 769008, India

A methodology has been developed to predict fatigue crack propagation life of 7020 T7 and 2024 T3 aluminum alloys under constant amplitude loading interspersed with mode-I spike overload. It has been assessed by adopting adaptive neuo-fuzzy inference system (ANFIS), a novel soft-computing approach, suitable for non-linear, noisy and complex problems like fatigue. The proposed model has proved its efficiency quite satisfactorily compared to authors' previously proposed 'Exponential Model', when tested on both the alloys.

Keywords: **A**daptive neuro-fuzzy inference system; Adaptive network; Delay cycle; Exponential model; Fatigue crack growth rate; Fatigue life; Retardation parameters.

* Corresponding author. Tel.: +91 661 2464553 (J. R. Mohanty)

Email address: guddy95@yahoomail.co.in, guddy95@gmail.com,

Nomenclature

a	crack length (mm) measured from the edge of the plate
a_{i}	crack length corresponding to the 'i^{th}' step (mm)
a_{j}	crack length corresponding to the 'j^{th}' step (mm)
$a_{\mathrm{d}}^{\mathrm{AN}}$	retarded (ANFIS) crack length (mm)
$a_{\mathrm{d}}^{\mathrm{EN}}$	retarded (exponential) crack length (mm)
$a_{\mathrm{d}}^{\mathrm{E}}$	retarded (experimental) crack length (mm)
$A,\ B,\ C$	fuzzy sets
$A_{\mathrm{j}},\ B_{\mathrm{k}},\ C_{\mathrm{m}}$	linguistic labels
A', B', C' and D'	curve fitting constants in the 'Exponential Model'
$\mathrm{d}a/\mathrm{d}N$	crack growth rate (mm/cycle)
E	Young's modulus (MPa)
f	linear consequent function of TSK model
$K_{\max}$	maximum stress intensity factor ($\mathrm{MPa}\sqrt{\mathrm{m}}$)
ΔK	stress intensity factor range ($\mathrm{MPa}\sqrt{\mathrm{m}}$)
K_{C}	plane stress fracture toughness ($\mathrm{MPa}\sqrt{\mathrm{m}}$)
K_{ol}	stress intensity factor at overload point ($\mathrm{MPa}\sqrt{\mathrm{m}}$)
$K_{\max}^{\mathrm{B}}$	maximum base line stress intensity factor ($\mathrm{MPa}\sqrt{\mathrm{m}}$)
l	dimensionless factor in the 'Exponential Model' formulation
m	specific growth rate
m_{ij}	specific growth rate corresponding to the step interval i-j
n	No. of input nodes
N_{i}	number of cycles corresponding to the 'i^{th}' step
N_{j}	number of cycles corresponding to the 'j^{th}' step
N_d^{AN}	number of delay (ANFIS) cycles
$N_{\mathrm{d}}^{\mathrm{EN}}$	number of delay (exponential) cycles
$N_{\mathrm{d}}^{\mathrm{E}}$	number of delay (experimental) cycles

N_f^{AN}	number of delay (ANFIS) cycles
$N_{\mathrm{f}}^{\mathrm{EN}}$	final (exponential) number of cycles
$N_{\mathrm{f}}^{\mathrm{E}}$	final (experimental) number of cycles
o, p, q, r	consequent parameters
p	No. of fuzzy partitions
S_1, S_2, S_3	universe of discourse of three input variables
w	plate width (mm)
w_i	firing strength
x_1, x_2, x_3	input variables of ANFIS
β	overloading angle
$\mu_{A_j}(x_1), \mu_{B_k}(x_2), \mu_{C_m}(x_3)$	membership grade functions
σ_{ys}	yield point stress (MPa)

1. Introduction

The use of high strength materials is common in aircrafts, ships and offshore structures which are sensitive to flaws and defects. Those tiny flaws or imperfections are present to some extent during manufacturing as fabrication defects or material defects (in the form of inclusions or second phase particles) or localized damage in service. They eventually coalesce and develop into larger cracks and subsequently grow to a critical size leading to catastrophic failure of the structure. The structural components are often designed for some degree of damage tolerance to ensure survival in the presence of growing cracks. The basic need of damage tolerance design philosophy is to establish a timely inspection schedule so as to give the inspector the ample opportunities to detect a growing crack. It helps in recommending the repair or replacement of the affected component in order to prevent failure, injury or loss of life and thus reduce any associated financial loss. These all need a reliable life prediction methodology.

Load sequence is one of the major factors that affect the fatigue crack growth rate particularly in case of variable amplitude loading (VAL). The simplest type of VAL is the occurrence of high peak loads interspersed in constant amplitude loading (CAL) history. Typical examples where this type of load interaction occurs are airplane flying under gust spectrum, ships and offshore structures coming under high loads for a certain periods etc. When such types of load sequence are tensile in nature the crack growth is slowed down in comparison to the normal (CAL) growth rate leading to retardation in fatigue crack growth. The assessment of life under those complex situations is certainly tedious because of the lack of proper understanding of micro-mechanisms of retardation. Based on various mechanisms, a number of retardation models (Willenborg, Engle & Wood, 1971; de Koning, 1981; Bolotin & Lebedev, 1996; Lee, Kim & Nam, 2003; Borrego, Ferreira, Pinho & Costa, 2003; Kim & Sim, 2003) have been proposed till date. However, each model has its own merits and demerits as a result; significant ambiguities and disagreements still exist in terms of the exact mechanism of retardation (Sadananda, Vasudevan, Holtz & Lee, 1999; Murthy, Palani & Iyer, 2004).

With the recent advances in the field of soft-computing technology, crack propagation life is now being simulated with the existing experimental data so as to avoid

more difficult, time-consuming and costly fatigue tests. Out of different soft-computing methods such as artificial neural network (ANN), genetic algorithm (GA), fuzzy-logic, adaptive neuo-fuzzy inference system (ANFIS) etc, ANFIS is one of the recent developed method to handle fatigue problems successfully. Although ANN has been frequently used by several researchers (Pleune & Chopra, 2000; Venkatesh & Rack, 1999; Cheng, Huang & Zhou, 1999; Pidaparti & Palakal, 1995; Jia & Davalos, 2006) in modeling and analyzing different types of fatigue problems during last 10 years, the application of other soft-computing techniques are quite rare. Canyurt (Canyurt, 2004) has developed a genetic algorithm fatigue strength estimation model (GAFSEM) to estimate the fatigue strength of the adhesively bonded tubular joint using several adherent materials. Bukkapatnam and Sadananda (Bukkapatnam and Sadananda, 2005) have predicted fatigue crack growth life of Al 5052 by using genetic algorithm in the light of 'Unified Approach' with a prediction result of 12% error. In the later stage, this innovative modeling tool has been used in modeling the fatigue life of several fiber-reinforced composite material systems by Vassilopoulos & Bedi (Vassilopoulos & Bedi, 2008). Wu et al. (Wu, Hu & Pecht, 1990) has applied fuzzy regression analysis to analyze the fatigue crack growth data and shown that the result is quite comparable with the conventional least square methods. As far as the application of adaptive neuo-fuzzy inference system (ANFIS) in the field of fatigue is concerned, very limited work has been reported in literature (Vassilopoulos & Bedi, 2008; Jarrah, Al-Assaf & El Kadi, 2002). Both ANN and fuzzy logic techniques have their own advantages and disadvantages. However, ANFIS combines the advantages of both the techniques without having any of their disadvantages.

The focus of the present investigation is on the development of a novel life prediction model using ANFIS in case of constant amplitude loading interspersed with mode-I spike overload. The model result has been compared with the results of 'Exponential Model' earlier proposed by the authors (Mohanty, Verma & Ray, 2009). It has been observed that the present model not only evaluates different retardation parameters but also predicts the end life of both 7020T7 and 2024T3 Al-alloys quite satisfactorily.

2. Adaptive neuro-fuzzy inference system (ANFIS)

Adaptive Network based Fuzzy Inference System (ANFIS) is a cross between an artificial neural network (ANN) and a fuzzy inference system (FIS). It is a powerful universal approximator that removes the requirement for manual optimization of the fuzzy system by automatically tuning the system parameters using neural network technique. It combines advantages of both ANN and FIS, thereby improving the system performances without operator intervention. With a given input/output data set, this integrated neuro-fuzzy system constructs a fuzzy inference system whose membership function parameters are tuned (adjusted) using either a back-propagation algorithm alone, or in combination with least-squares estimator. Before applying the above novel computational technique one needs to be familiar with its fundamental principle as discussed in the following sections.

2.1 Fuzzy Inference System (FIS)

Fuzzy inference systems also called rule-based systems are capable modeling non-linear complex problems by employing both fuzzy logic and linguistic if-then rules. A simple model of the system is presented in Fig. 1. The controller has four main components: the fuzzification interface, inference engine, rule base and defuzzifier. The rule base contains a number of linguistic fuzzy if-then rules provided by experts. The fuzzification interface transforms crisp inputs into corresponding fuzzy memberships in order to activate rules that are in terms of linguistic variables. The inference engine defines mapping from input fuzzy sets into output fuzzy sets. The defuzzifier transforms the fuzzy results into a crisp output through various defuzzyfication methods including the centroid, maximum, mean of maxima, height and modified height defuzzifier. The two commonly used inference techniques are Mamdani (Mamdani & Assilian, 1975) and Takagi-Sugeno (TSK) (Takagi & Sugeno, 1985). In the present investigation, type-3 ANFIS (Jang, 1993) topology based on first-order Takagi-Sugeno (TSK) if-then rules has been used, where the output is a first-order polynomial and the fuzzy rules of the output is represented by a crisp function.

2.2 Adaptive Network

An adaptive network is a multilayer feed-forward neural network with supervised learning in which each node performs a particular function (node function) on incoming

signals. The detail description of the procedure has been cited by Jang (Jang, 1993). It is a network structure consisting of both circles (fixed) and square (adaptive) nodes connected by directional links showing direction of signals between nodes. The parameter set of an adaptive network is the union of the parameter sets which are updated according to the given training data and a gradient based learning procedure.

2.3 Structure of ANFIS

The illustration of ANFIS structure used in the present work is given in Fig. 2 which is a first-order Takagi-Sugeno type. The network calculates the system's output for given input data set through fuzzy if-then rules. The optimal model parameters are determined by both back-propagation and hybrid learning algorithms. A typical first-order TSK fuzzy inference system with three inputs and one output can be expressed in the following form:

IF x_1 is A_j (1)

x_2 is B_k (2)

AND x_3 is C_m (3)

THEN $f_i = o_i x_1 + p_i x_2 + q_i x_3 + r_i$ (4)

for $j = 1,...., S_1$

$k = 1,...., S_2$

$m = 1,...., S_3$

$i = 1,...., S_1 \times S_2 \times S_3$

where *A*, *B*, and *C* are fuzzy sets defined on input variables x_1, x_2, and x_3 respectively; S_1, S_2, and S_3 are the number of membership functions; *f* is a linear consequent function defined in terms of input variables; while *o*, *p*, *q*, and *r* are linear coefficients referred to as consequent parameters. It consists of a number of interconnected fixed and adjustable nodes and is composed of five layers having three inputs and one output. The functions of different layers are as follows:

Layer-1: Every node in this layer is a square node with a particular membership function specifying the degree to which a given input satisfies the quantifier. For three inputs ANFIS model, the output of a given node is given by:

$$O_j^1 = \mu_{A_j}(x_1), \quad j = 1,....., S_1 \tag{5}$$

$$O_k^1 = \mu_{B_k}(x_2), \quad k = 1,....., S_2 \tag{6}$$

$$O_m^1 = \mu_{C_m}(x_3), \quad m = 1,....., S_3 \tag{7}$$

where S_1, S_2, and S_3 are universes of discourse of three input variables respectively; x is the input to nodes j, k, and m respectively; A_j, B_k, and C_m are the linguistic labels (small, large etc) associated with the respective node functions. In this layer, the membership function can be any appropriate parameterized membership function such as triangular, Gaussian or bell. Bell membership function has been selected for the present work because, it has the characteristics of smoothness and succinctness, and are extensively applied to the fuzzy sets. It is defined as:

$$\mu_{A_i}(x) = \frac{1}{1 + \left\{ \frac{x - c_i}{a_i} \right\}^{b_i}} \tag{8}$$

where a_i, b_i, and c_i are the membership function parameters. Parameters in this layer are referred to as 'premise parameters'.

Layer-2: Every node in this layer is a fixed node, marked by a circle, whose output is the product of all the incoming signals (T-norm operation):

$$O_i^2 = w_i = \mu_{A_j}(x_1)\mu_{B_k}\mu_{C_m} \tag{9}$$

The output of a node in the 2nd layer represents the firing strength (degree of fulfillment) of the associated rule. Typical representation of fuzzy rules in a first-order TSK FIS is given as:

Rule-1: if x_1 is A_1, x_2 is B_1 and x_3 is C_1 then $f_1 = o_1x_1 + p_1x_2 + q_1x_3 + r_1$ (10)

Rule-2: if x_1 is A_2, x_2 is B_2 and x_3 is C_2 then $f_2 = o_2x_1 + p_2x_2 + q_2x_3 + r_2$ (11)

Layer-3: Every node in this layer is also a circle node. The output of i^{th} node is the ratio of the i^{th} rule's firing strength to the sum of all rules' firing strengths:

$$O_i^3 = \overline{w}_i = \frac{w_i}{w_1 + w_2 + w_3} \tag{12}$$

The output is called as 'normalized firing strength'.

Layer-4: Every node i in this layer is a square or adaptive node with a node function:

$$O_i^3 = \overline{w}_i f_i = \overline{w}_i \left(o_i x_1 + p_i x_2 + q_i x_3 + r_i\right) \tag{13}$$

where $\overline{w}_i$ is the output of layer 3, and $\{o_i, p_i, q_i, r_i\}$ is the parameter set. Parameter in this layer is referred to as the consequent parameter.

Layer-5: The single node in this layer computes the overall output as the summation of all incoming signals:

$$O_i^5 = \sum_i \overline{w}_i f_i = \frac{\sum w_i f_i}{\sum w_i} \tag{14}$$

In the proposed ANFIS topology, there are S_1, S_2 and S_3 number of membership functions associated with each of the three inputs respectively. So the input space is partitioned into $(S_1 \times S_2 \times S_3)$ fuzzy subspaces, each of which is governed by fuzzy if-then rules. The premise part of a rule (layer 1) defines a fuzzy sub-space, while the consequent part (layer 4) specifies the output within this sub-space.

2.4 Learning algorithm of ANFIS

The basic learning rule of adaptive network is back-propagation algorithm where the model parameters are updated by a gradient descent optimization technique. However, due to the slowness and tendency to become trapped in local minima its application is limited. A hybrid-learning algorithm, on the other hand is an enhanced version of the back-propagation algorithm. It is applied to adapt the premise and consequent parameters to optimize the network. In the forward pass, functional signals go forward till layer 4 and the consequent parameters are identified by the least square estimate. In the backward pass, the error rates propagate backward and the premise parameters are updated by the gradient descent method. Heuristic rules are used to guarantee fast convergence. The details of the above technique have been elaborately discussed by Jang (Jang, 1993).

3. Experimental data base

The present work has been focused to predict the residual fatigue life along with various retardation parameters of two aluminum alloys (7020 T7 and 2024 T3) under single tensile overload in mode-I by applying ANFIS model. For the purpose, the experimental data base was created from the fatigue tests conducted by the present authors' (Mohanty, Verma & Ray, 2009) in their earlier work. Single edge notch tension

(SEN) specimens cut from a 6.5mm plate in an LT plane (with the loading aligned in the longitudinal direction) were subjected to single spike overload (loading rate of 8KN/min) at an *a*/*w* ratio of 0.4 followed by constant amplitude load test. The various overload ratios $\left(R_{ol} = {K_{ol}}/{K^{B}_{\max}} \right)$ for the two alloys were as follows:

Al 7020 T7: 2.0, 2.25, 2.35, 2.5, 2.6 and 2.75

Al 2024 T3: 1.5, 1.75, 2.0, 2.1, 2.25 and 2.5

All the fatigue tests were performed in a servo-hydraulic controlled dynamic testing machine *Instron-8502* (250KN load capacity) in ambient air at room temperature with a frequency of 6Hz maintaining a load ratio of 0.1.

4. Design of ANFIS model for crack growth rate prediction

It has been verified earlier (Willenborg, Engle & Wood, 1971; de Koning, 1981; Bolotin & Lebedev, 1996; Lee, Kim & Nam, 2003; Borrego, Ferreira, Pinho & Costa, 2003; Kim & Sim, 2003; Mohanty, Verma & Ray, 2009) that the application of a single tensile overload during fatigue crack propagation can lead to significant retardation of crack growth and results in an increase in the specimen life time (Fig. 3 and 4). This delaying effect must be taken into account while predicting the residual fatigue crack growth lives of the structures subjected to variable amplitude loading conditions. Not only the enhanced residual life, but various retardation parameters such as number of delay cycles (N_{d}), retarded crack length (a_{d}) etc are also equally important for quantitative analysis of the retardation effect. This is, of course, one of the important factors of damage tolerant design philosophy adopted in various air-craft industries. Hence, the present work has been devoted for automatic prediction of the above quantities quantitatively by using neuro-fuzzy technique.

The most fundamental principle of ANFIS is that the input/output data must be normalized (pre-processing) before applying the model to obtain optimum results. It should be pointed out that in case of single tensile overload; crack growth retardation depends on the magnitude of overload ratio (R_{ol}). Further, it has been proved that fatigue crack growth rate is governed not only by single crack driving force ΔK, but, according to 'Unified Approach', by the simultaneous action of both ΔK and $K_{\max}$ (Sadananda, Vasudevan, Holtz & Lee, 1999; Dinda & Kujawski, 2004; Noroozi, Glinka

& Lambert, 2005). Therefore, overload ratio (R_{ol}), maximum stress intensity factor (K_{max}), and stress intensity factor range (ΔK) were considered as linguistic input variables whereas, crack growth rate (da/dN) was taken as output variable for the proposed model. Out of six sets of overload test data (R_{ol} = 2.0, 2.25, 2.35, 2.5, 2.6 and 2.75 for Al 7020 T7 and 1.5, 1.75, 2.0, 2.1, 2.25 and 2.5 for Al 2024 T3) one set for each alloys i.e. R_{ol} = 2.35 for Al 7020 T7 and R_{ol} = 2.1 for Al 2024 T3 was selected as the validation set (VS). The other five data sets were considered as training set (TS). The input variables i.e. overload ratio, maximum stress intensity factor and stress intensity factor range were conditioned in such a way that their maximum values were normalized to unity. The crack growth rate, which constitutes the system output, was also normalized in similar manner.

Referring to Fig. 2, layer 1 has 15 (5×3) nodes with 45 parameters. Layers 2, 3 and 4 have 125 (5^3) nodes each with 500 parameters associated in layer 4. The performances of the model during training and testing were assessed using various standard statistical performance evaluation criteria such as root mean square error (RMSE); coefficient of determination (R^2) and mean percent error (MPE) defined by Eqs. 15 to 17:

$$RMSE = \left((1/p) \sum_{i=1}^{p} |t_i - o_i| \right)^{1/2} \tag{15}$$

$$R^2 = 1 - \left(\frac{\sum_{i=1}^{p} (t_i - o_i)^2}{\sum_{i=1}^{p} (o_i)^2} \right) \tag{16}$$

$$MPE = \frac{1}{p} \sum_{i=1}^{p} \left(\frac{t_i - o_i}{t_i} \times 100 \right) \tag{17}$$

where 't' is the target value, 'o' is the output value, and 'p' is the number of data items.

5. Results and discussion

5.1 Simulation results

In order to implement the ANFIS model (Fig. 2) in the present work, a computer program was performed under MATLAB environment using the Fuzzy Logic Toolbox. The numbers of membership functions (MF) were chosen to be 5-5-5

corresponding to the inputs R_{ol}, K_{max} and ΔK respectively. The $5\times5\times5=125$ fuzzy 'if-then' rules were constituted in which fuzzy variables were connected by T-norm (fuzzy AND) operators. The adjustment of premise and consequent parameters was made in batch mode based on the hybrid-learning algorithm. The model was trained for 4000 epochs until the given tolerance was achieved. The flow chart of the trained ANFIS model is illustrated in Fig. 5. Fig. 6 and 7 show the resulting surface plots identifying the relationship among selected variables. It can be observed from the surface plots that the identified relationship by ANFIS methodology is non-linear in nature. Fig. 8 shows the membership function diagrams of the inputs of the crack growth rate prediction process before training. Table 1 summarizes all the characteristics of ANFIS network used. The performance of the model during training and testing was verified through three statistical indices (Eqs. 15 to 17) and presented in Table 2.

Based on above statistical performances, the trained ANFIS model was tested for the validation sets (R_{ol} = 2.35 for Al 7020 T7 and R_{ol} = 2.10 for Al 2024 T3) and the predicted crack growth rates were compared with the experimental data in Figs. 9 and 10. The numbers of cycles (fatigue life) were calculated from predicted and experimental results in the excel sheet (Figs. 11 and 12) as per the following equation:

$$N_j = \frac{a_j - a_i}{da/dN} + N_i \tag{18}$$

where, a_i and a_j = crack length in i^{th} step and j^{th} step in 'mm' respectively,

N_i and N_j = No. of cycles in i^{th} step and j^{th} step respectively,

i = No. of experimental steps,

and $j = i+1$

5.2 Comparison with 'Exponential Model'

The predicted ANFIS results were quantitatively compared in Table 3 with 'Exponential Model' (Mohanty, Verma & Ray, 2009) results proposed earlier by the present authors. At this point, a brief overview of the exponential model needs to be discussed for clear understanding. The fundamental equations of the model were:

$$a_j = a_i e^{m_{ij}(N_j - N_i)} \tag{19}$$

$$m_{ij} = \frac{\ln\left(\frac{a_j}{a_i}\right)}{\left(N_j - N_i\right)} \tag{20}$$

where, a_i and a_j = crack length in i^{th} step and j^{th} step in 'mm' respectively,

N_i and N_j = No. of cycles in i^{th} step and j^{th} step respectively,

m_{ij}= specific growth rate in the interval *i-j*,

i = No. of experimental steps,

and $j = i+1$

The exponent *'m'*, called specific growth rate, was correlated with a parameter *'l'* which takes into account the two crack driving forces ΔK and K_{max} as well as material parameters K_C, E, σ_{ys} by the following equation:

$$m = A'l^3 + B'l^2 + C'l + D' \tag{21}$$

where, $l = \left[\left(\frac{\Delta K}{K_C}\right)\left(\frac{K_{max}}{K_C}\right)\left(\frac{\sigma_{ys}}{E}\right)\right]^{\frac{1}{4}}$

and A', B', C', D' are curve-fitting constants.

The values of specific growth rate (m) were obtained using equation (21) for all the overload ratios of both the alloys. It was observed that the above values were different for different overload ratios. This is due to the fact that the amount of retardation is solely dependent on the overload ratio values. Therefore, each constant of different overload ratios (except the tested R_{ol}) were correlated with R_{ol} by a 2nd degree polynomial curve fit through equations (22) to (29) as follows:

for Al 7020 T7:

$$A' = (45168\times10^{-6})R_{ol}^2 + (-354083\times10^{-6})R_{ol} + (460905\times10^{-6}) \tag{22}$$

$$B' = (-9600.8\times10^{-6})R_{ol}^2 + (81208\times10^{-6})R_{ol} + (-107645\times10^{-6}) \tag{23}$$

$$C' = (354.69\times10^{-6})R_{ol}^2 + (-4462.5\times10^{-6})R_{ol} + (6389.1\times10^{-6}) \tag{24}$$

$$D' = (3.6904\times10^{-6})R_{ol}^2 + (49.842\times10^{-6})R_{ol} + (-90.813\times10^{-6}) \tag{25}$$

and for Al 2024 T3:

$$A' = (-31269\times10^{-6})R_{ol}^2 + (127925\times10^{-6})R_{ol} + (-143543\times10^{-6}) \tag{26}$$

$$B' = (13117\times10^{-6})R_{ol}^2 + (-53849\times10^{-6})R_{ol} + (60396\times10^{-6}) \tag{27}$$

$$C' = (-1883\times10^{-6})R_{ol}^2 + (7761\times10^{-6})R_{ol} + (-8506.5\times10^{-6}) \quad (28)$$

$$D' = (86.669\times10^{-6})R_{ol}^2 + (-359.11\times10^{-6})R_{ol} + (385.94\times10^{-6}) \quad (29)$$

Putting the values of various constants in equation (15) the predicted *'m'* values were determined for the tested overload ratios (R_{ol} =2.35 for 7020 T7 and R_{ol} =2.10 for 2024 T3). Then the number of cycles (fatigue life) was calculated cycle-by-cycle basis as follows;

$$N_j = \frac{\ln\left(\frac{a_j}{a_i}\right)}{m_{ij}} + N_i \quad (30)$$

The various predicted model results are presented in Table 3 along with the experimental results for quantitative comparison. The graphs for *a*-*N* and d*a*/d*N*-Δ*K* are plotted in Figs. 13 to 16 for comparison of both the model results along with experimental findings. Figs. 17 to 20 show various retardation parameters in order to account for the retardation effect.

5.3 Analysis of results

The performances of different models were analyzed by comparing the prediction results with the experimental findings by the following criteria:

- Percentage deviation of predicted data from the experimental data i.e.
  $$\%\,\text{Dev} = \frac{\text{Predicted result} - \text{Experimental result}}{\text{Experimental result}} \times 100$$
- Prediction ratio which is defined as the ratio of actual result (i.e. experimental) to predicted result i.e.
  $$\text{Prediction ratio, } P_r = \frac{\text{Actual result}}{\text{Predicted result}}$$
- Error bands i.e. the scatter of the predicted life in either side of the experimental life within certain error limits.

Table 4 presents various model results as per the above evaluation criteria. From the above table it is observed that the percentage deviations of different retardation parameters are within $\pm 7.0\%$ (maximum). The post overload fatigue crack propagation lives are within –0.2% to +1.5% whereas, the prediction ratio is about 1.0. From the above results it can be concluded that the performance of ANFIS model is quite

satisfactorily. As far as relative performance is concerned, the exponential model gives better results in comparison to ANN model. Analyzing the error band scatter (Figs. 21 and 22) it is observed that the results of Al 7020 T7 are within $\pm 0.05\%$ error band while, it is less i.e. $\pm 0.025\%$ for Al 2024 T3.

5.4 Discussion

As shown in the Table 2, the MPE and RMSE values for the training data were negligible in both the cases. MPE values for testing were found to be slightly higher than those for training. The coefficient of determination was found to be close to 1.0 for training in both the materials. However, its value for testing was slightly less than unit. The performance of the proposed ANFIS model was quite good as coefficient of determination was high and errors were small. But one cannot rely only on those numerical values. It may sometimes happen that numerical values are good, but fitting results of the model are not good in some operating area. Therefore, the trained model was tested for validation data sets (VS) and the various predicted results were compared with the experimental findings as well as with the exponential model results presented in Table 3. It was observed that percentage errors of retarded crack lengths (a_d) in case of both the materials were within +7%, whereas the percentage error of retarded number of cycles (N_d) were maximum of +8%. As far as the end lives of the specimens were concerned, the error percentage was limited to maximum of +2%. Although the accuracy of the proposed model was low in comparison to exponential model, but it was within the acceptable range. This is due to the fact that prediction accuracy of fatigue, in general, is quite low. Moreover, determination of various curve-fitting constants from the scattered experimental fatigue data in the exponential model is a tedious job in comparison to the formulation of fuzzy rules in ANFIS model, which is one of its advantages.

Limitation of neuro-fuzzy modeling is that selection of the number of parameters affects the goodness and adaptiveness of the model. For example too few parameters neglect non-linearities of the process affecting the model performance. On the contrary, too many parameters may cause overfitting. Hence, the number of parameters should be suitable for the model to work well for both training and testing data. Further, the neuro-fuzzy model can only be used in the training range.

6. Summary and conclusion

Prediction of fatigue crack propagation life is a prime requirement in order to avoid costly and time consuming fatigue tests. It provides prior warning to repair/replace the damaged machine parts in time so as to avoid catastrophic failure. But, it is obviously is a challenging job to the fatigue communities because, the physical interpretation of fatigue damage is quite ambiguous since it depends on several mechanisms. Further, there are so many factors responsible for the fatigue cracks to propagate. Therefore, formulation of a universal mathematical model for fatigue life prediction to suit for all the situations is almost impossible. Recently, introduction of various soft-computing techniques in the field of fatigue solves the above complex problems in a much better way.

In the present work, the adaptive neuro-fuzzy inference system (ANFIS), a novel non-conventional hybrid technique was applied to predict various retardation parameters along with residual fatigue life under the given loading condition. The performance of the proposed model was compared with the results of exponential model for two aluminum alloys. It was observed that its prediction accuracy was quite reasonable. As a future work, the above method can be successfully applied to determine the specific growth rate (m) of the exponential model which in turn, the prediction of fatigue life (No. of cycles) will be possible by avoiding the calculation of various curve-fitting constants.

References

Bolotin, V.V., & Lebedev, V.L. (1996). Analytical model of fatigue crack growth retardation due to overloading. International Journal of Solids and Structure, 33(9), 1229–1242.

Borrego, L.P., Ferreira, J.M., Pinho, da., Cruz, J.M., & Costa, J.M. (2003). Evaluation of Overload Effects on Fatigue Crack Growth and Closure. Engineering Fracture Mechanics, 70, 1379–1397.

Bukkapatnam, S.T.S., & Sadananda, K. (2005). A genetic algorithm for unified approach-based predictive modeling of fatigue crack growth. International Journal of Fatigue, 27, 1354-1359.

Cheng, Y., Huang, W.L., & Zhou, C.Y. (1999). Artificial neural network technology for

the data processing of on-line corrosion fatigue crack growth monitoring. International Journal of Pressure Vesssel and Piping, 76, 113–116.

Canyurt, O.E. (2004). Fatigue strength estimation of adhesively bonded tubular joint using genetic algorithm approach. International Journal of Mechanical Science, 46, 359-370.

de Koning, A.U. (1981). A Simple Crack Closure Model for Prediction of Fatigue Crack Growth Rates under Variable-amplitude Loading. ASTM STP, 743, 63-85.

Dinda, S., & Kujawski, D. (2004). Corelation and prediction of fatigue crack growth for different R-ratios using K_{max} and ΔK^{+} parameters. Engineering Fracture Mechanics, 71(12), 1779-1790.

Jang, J.S.R. (1993). ANFIS: adaptive-network-based fuzzy inference systems. IEEE Transction, System Man and Cybernetics, 23, 665–685.

Jarrah, M.A., Al-Assaf, Y., & El Kadi, H. (2002). Neuro-fuzzy modeling of fatigue life prediction of unidirectional glass fiber / epoxy composite laminates. Journal of Composite Material, 36(6), 685–699.

Jia, J., & Davalos, J.F. (2006). An artificial neural network for the fatigue study of bonded FRP-wood interfaces. Composite Structure, 74, 106-114.

Kim, J.K., & Sim, D.S. (2003). A Statistical Approach for Predicting the Crack Retardation Due to a Single Tensile Overload. International Journal of Fatigue, 25, 335–342.

Lee, B.L., Kim, K.S., & Nam, K.M. (2003). Fatigue analysis under variable amplitude loading using an energy parameter. International Journal of Fatigue, 25, 621–631.

Mamdani, E.H., & Assilian, S. (1975). An experiment in linguistic synthesis with a fuzzy logic controller. International Journal of Man-Machine Studies, 7(1), 1–13.

Murthy, A.R.C., Palani, G.S., & Iyer, N.R. (2004). State-of-the-art review on fatigue crack growth analysis under variable amplitude loading. Institution of Engineers (India) Journal-CV, 85, 118-129.

Mohanty, J.R., Verma, B.B., & Ray, P.K. (2009). Prediction of fatigue crack growth and residual life using an exponential model: Part II (mode-I overload induced retardation). International Journal of Fatigue, 31, 425-432.

Noroozi, A.H., Glinka, G., & Lambert, S. (2005). A two parameter driving force for

fatigue crack growth analysis. International Journal of Fatigue, 27, 1277-1296.

Pidaparti, R.M.V., & Palakal, M.J. (1995). Neural Network Approach to Fatigue- Crack-Growth Predictions under Aircraft Spectrum Loadings. Journal of Aircraft, 32(4), 825-831.

Pleune, T.T., & Chopra, O.K. (2000). Using artificial neural networks to predict the fatigue life of carbon and low-alloy steels. Nuclear Engineering Design, 197, 1–12.

Sadananda, K., Vasudevan, A.K., Holtz, R.L., & Lee, E.U. (1999). Analysis of overload effects and related phenomenan. International Journal of Fatigue, 21, S233– S246.

Takagi, T., & Sugeno, M. (1985). Fuzzy identification of systems and its applications to modeling and control. IEEE Transction of System Man Cybernetics, 15, 116–132.

Venkatesh, V., & Rack, H.J. (1999). A neural network approach to elevated temperature creep-fatigue life prediction International Journal of Fatigue, 21, 225–234.

Vassilopoulos, A.P., & Bedi, R. (2008). Adaptive neuro-fuzzy inference system in modeling fatigue life of multidirectional composite laminates. Computational Material Science, 43(4), 1086-1093.

Willenborg, J.D., Engle, R.M., & Wood, H.A. (1971). A Crack Growth Retardation Model using an Effective Stress Concept. AFFDL, TM-71-1- FBR, Air Force Flight Dynamics Laboratory, Wright Patterson Airforce Base, OH.

Wu, X., Hu, J.M., & Pecht, M. (1990). Fuzzy Regression Analysis for Fatigue Crack Growth. TH0334-3/90/0000/0437$01 .OO, IEEE:437-40.

Table 1 – Characteristics of the ANFIS network

Type of membership function	generalized bell
Number of input nodes (n)	3
Number of fuzzy partitions of each variable (p)	5
Total number of membership functions	15
Number of rules $\left(p^n\right)$	125
Total number of nodes	394
Total number of parameters	545
Number of epochs	4000
Step size for parameter adaptation	0.01

Table 2 – Statistical performance of ANFIS model

Material	During training			During testing			Computat-ional Time (Min.)
	RMSE	R^2	MPE	RMSE	R^2	MPE	
7020 T7	0.002643	0.99873	0.348387	0.010879	0.96895	0.86495	355
2024 T3	0.001413	0.99967	0.385620	0.018268	0.93879	0.89697	425

Table 3 – Comparison of ANFIS and exponential model results with experimental data

Test sample	$a_{\mathrm{d}}^{\mathrm{AN}}$ mm	a_d^{EN} mm	$a_{\mathrm{d}}^{\mathrm{E}}$ mm	$N_{\mathrm{d}}^{\mathrm{AN}}$ K cy.	N_d^{EN} K cy.	$N_{\mathrm{d}}^{\mathrm{E}}$ K cy.	$N_{\mathrm{f}}^{\mathrm{AN}}$ K cy.	N_f^{EN} K cy.	$N_{\mathrm{f}}^{\mathrm{E}}$ K cy.
7020 T7	2.23	2.10	2.13	31.88	29.89	30.51	82.39	79.46	80.82
2024 T3	2.33	2.06	2.18	40.58	36.65	37.60	138.31	135.75	136.80

Table 4 – Various model results under interspersed mode-I overload

Test sample	% Dev a_d^{EN}	% Dev $a_{\mathrm{d}}^{\mathrm{AN}}$	% Dev N_d^{EN}	% Dev $N_{\mathrm{d}}^{\mathrm{AN}}$	% Dev N_f^{EN}	% Dev $N_{\mathrm{f}}^{\mathrm{AN}}$	Prediction ratio of exponential model P_r^{EN}	Prediction ratio of ANFIS P_r^{AN}
7020 T7	–0.80	–5.72	–1.20	+0.966	–0.241	+0.357	1.0024	0.996
2024 T3	–1.13	–6.52	–2.27	+1.653	–0.219	+0.604	1.0021	0.994

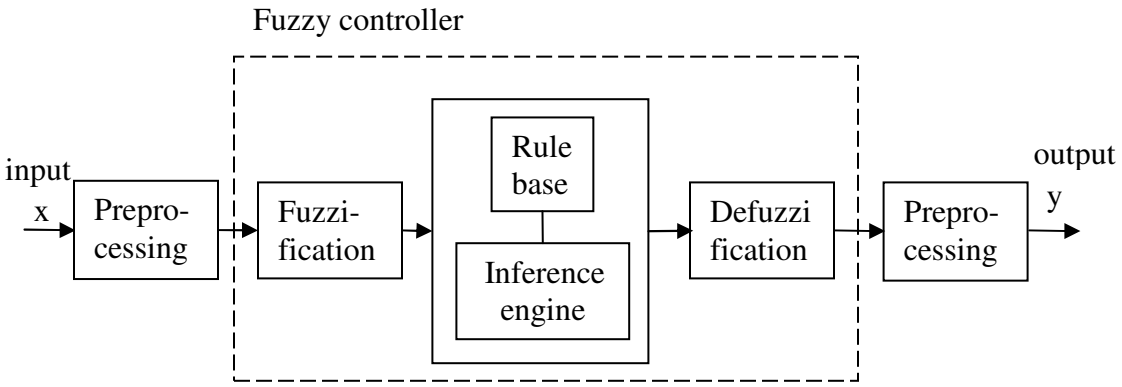

Fig. 1 – Fuzzy Inference System

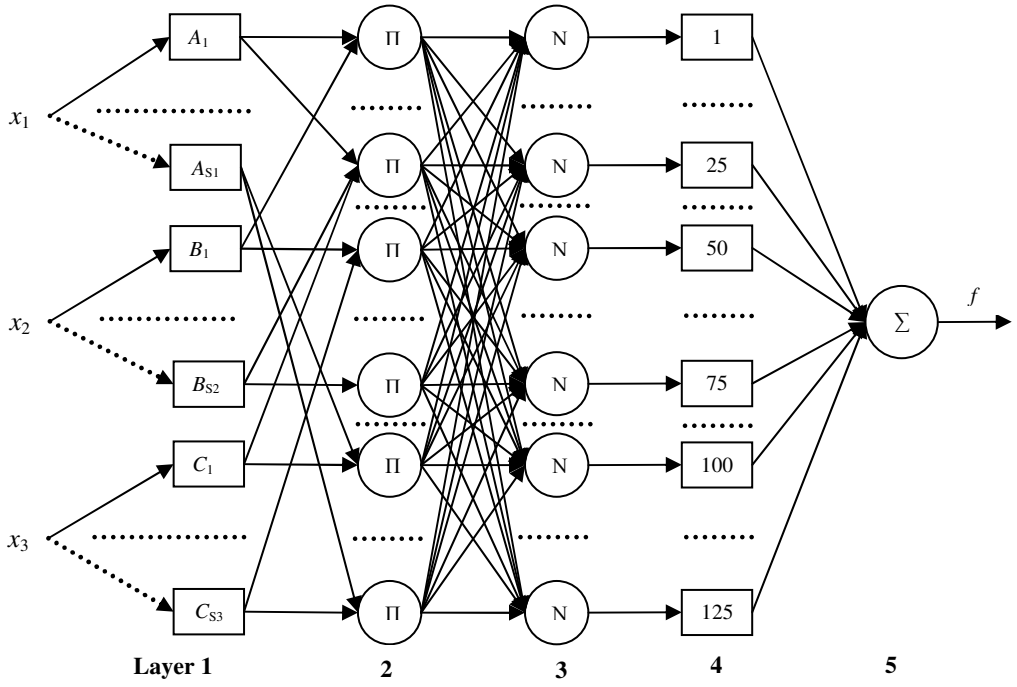

Fig. 2 – Structure of the ANFIS model

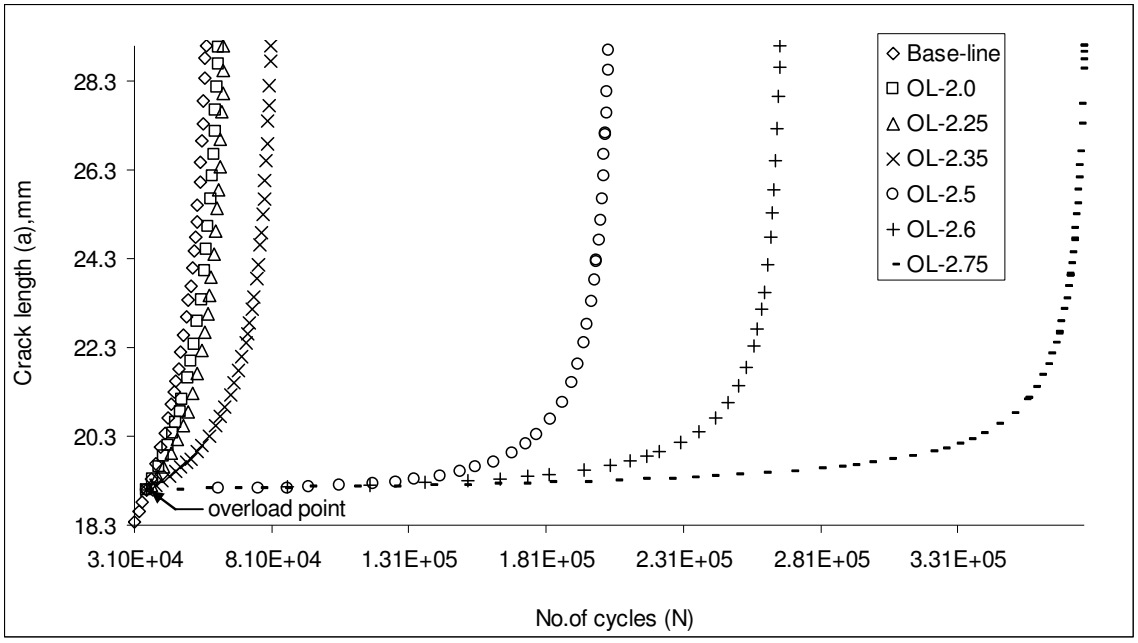

Fig. 3 – Superimposed $a \sim N$ curve of Al 7020 T7

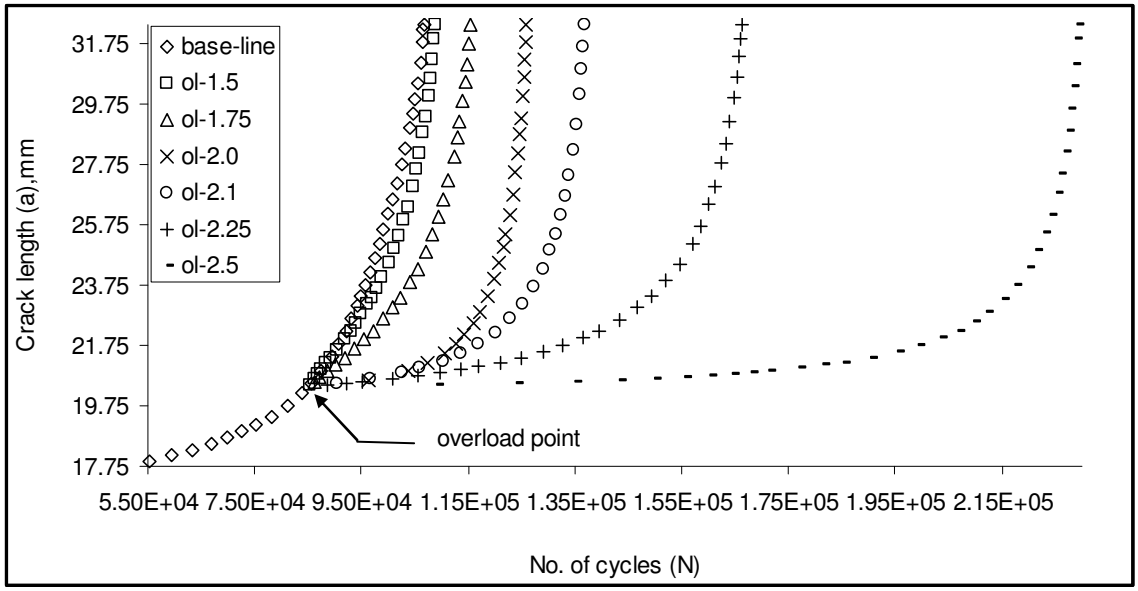

Fig. 4 – Superimposed $a \sim N$ curve of Al 2024 T3

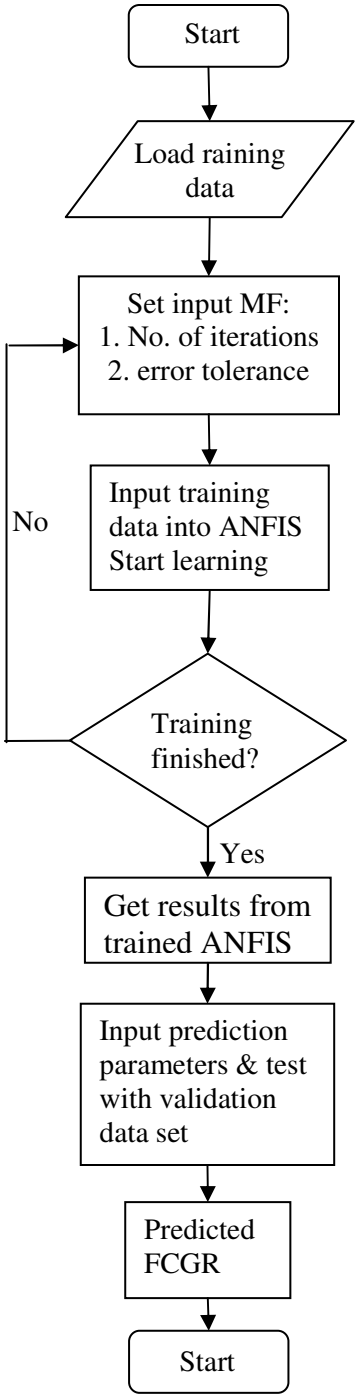

Fig. 5 – Flow chart of ANFIS model

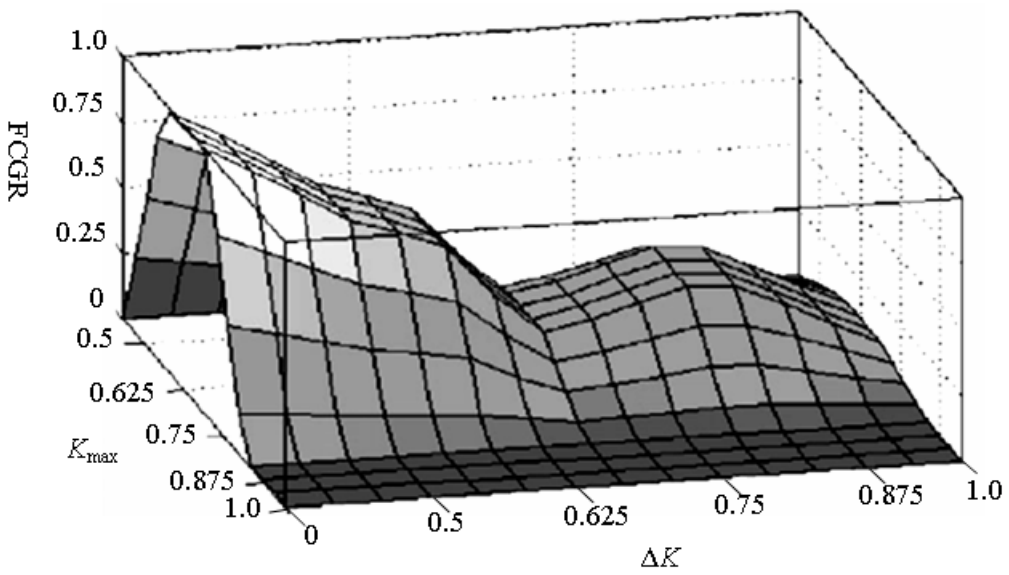

Fig. 6 – Surface plot for K_{max} and ΔK with FCGR of ANFIS model

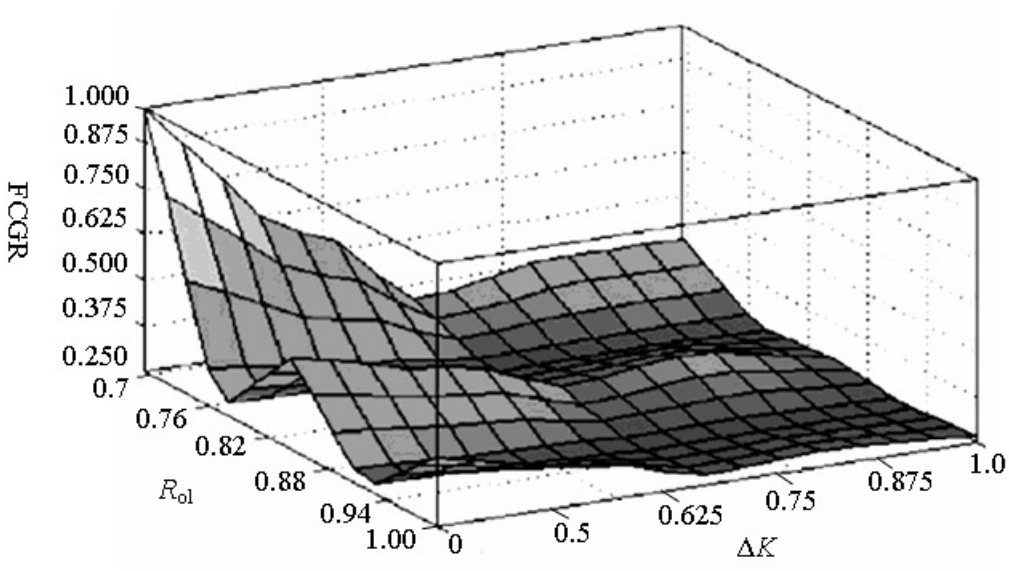

Fig. 7 – Surface plot for R_{ol} and ΔK with FCGR of ANFIS model

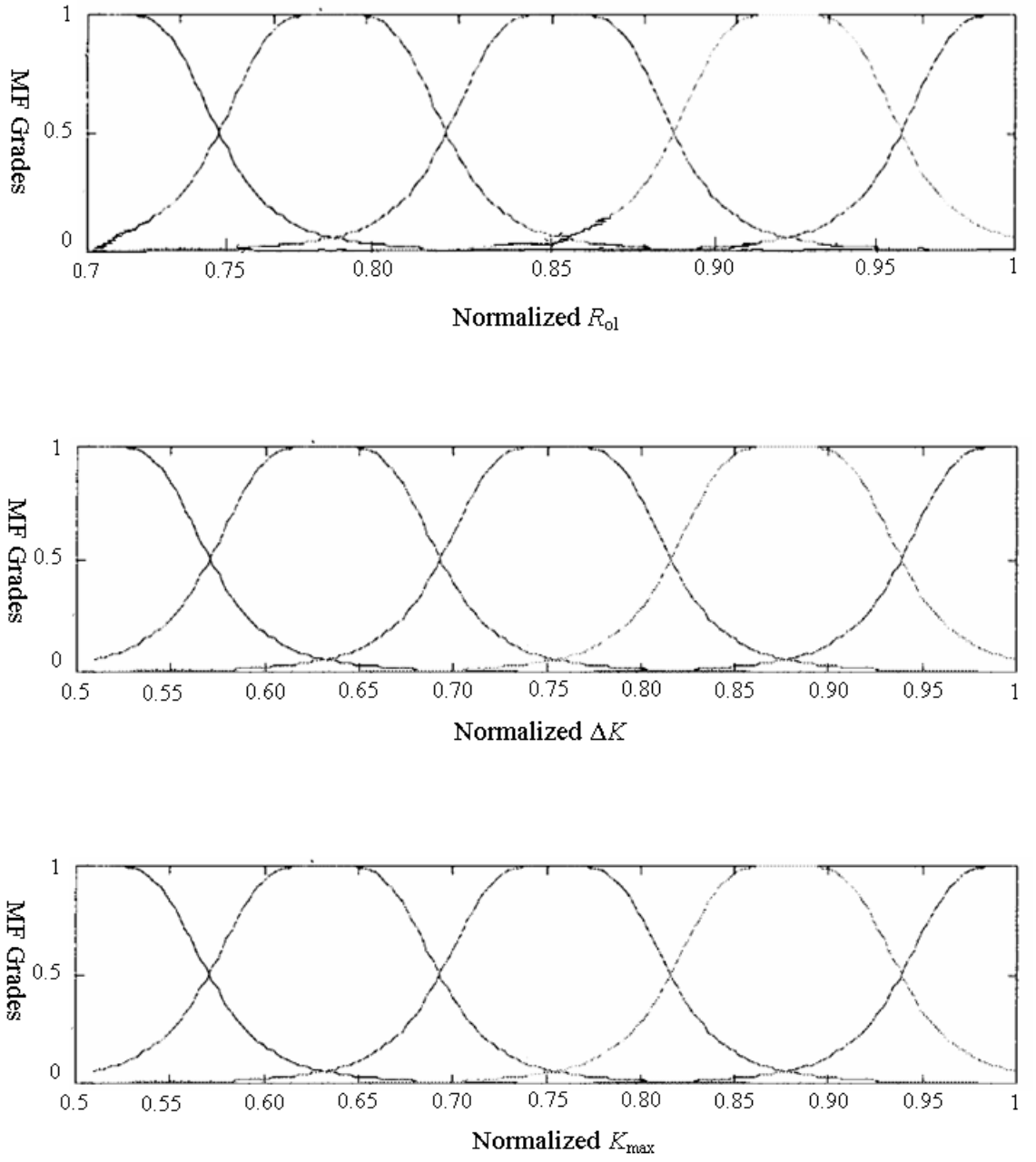

Fig. 8 – Bell-shaped membership functions of inputs before training

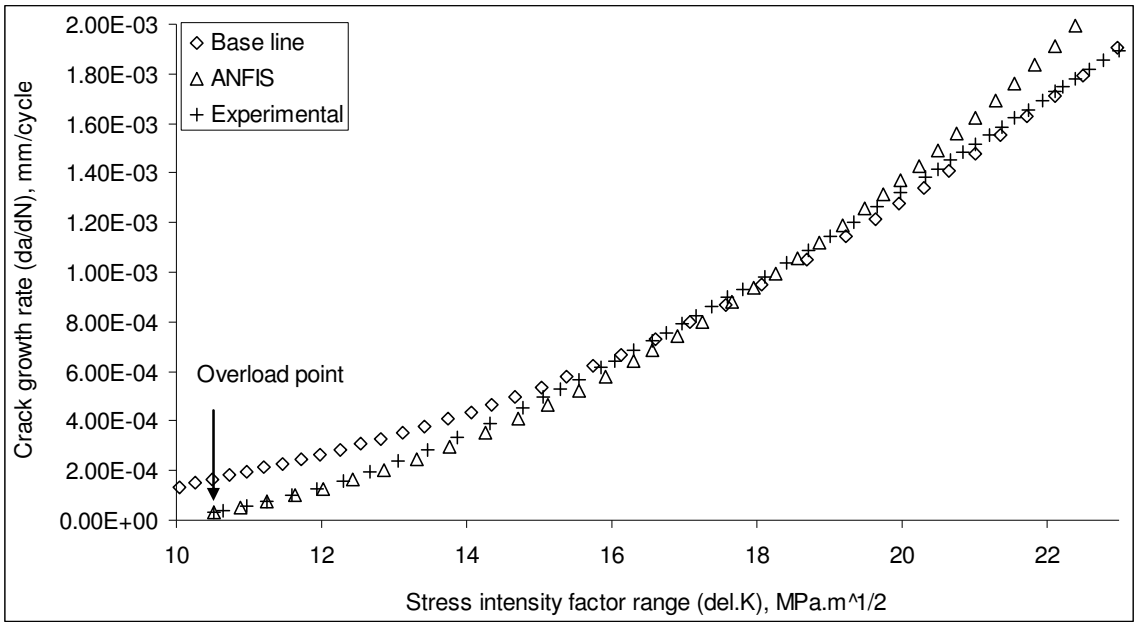

Fig. 9 – Comparison of predicted (ANFIS) and experimental crack growth rate with stress intensity factor range for Al 7020 T7

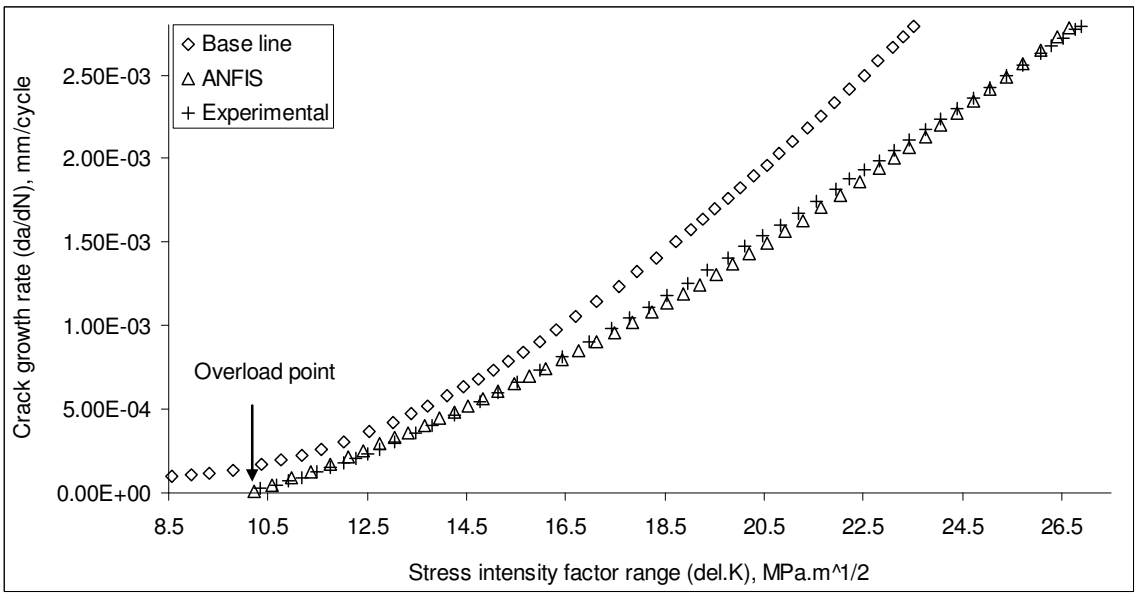

Fig. 10 – Comparison of predicted (ANFIS) and experimental crack growth rate with stress intensity factor range for Al 2024 T3

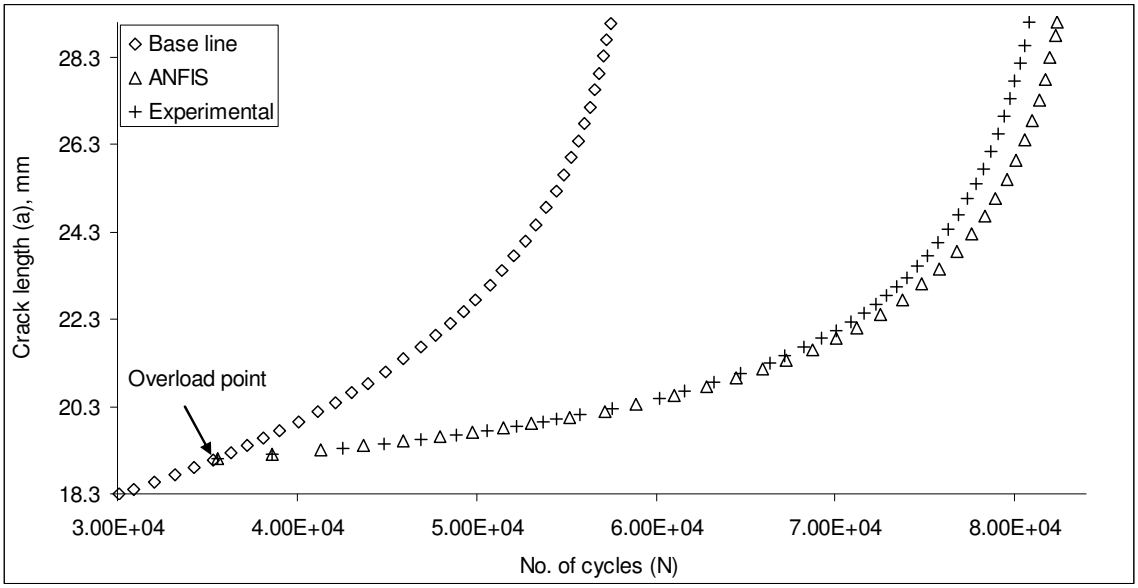

Fig. 11 – Comparison of predicted (ANFIS) and experimental crack length with number of cycle for Al 7020 T7

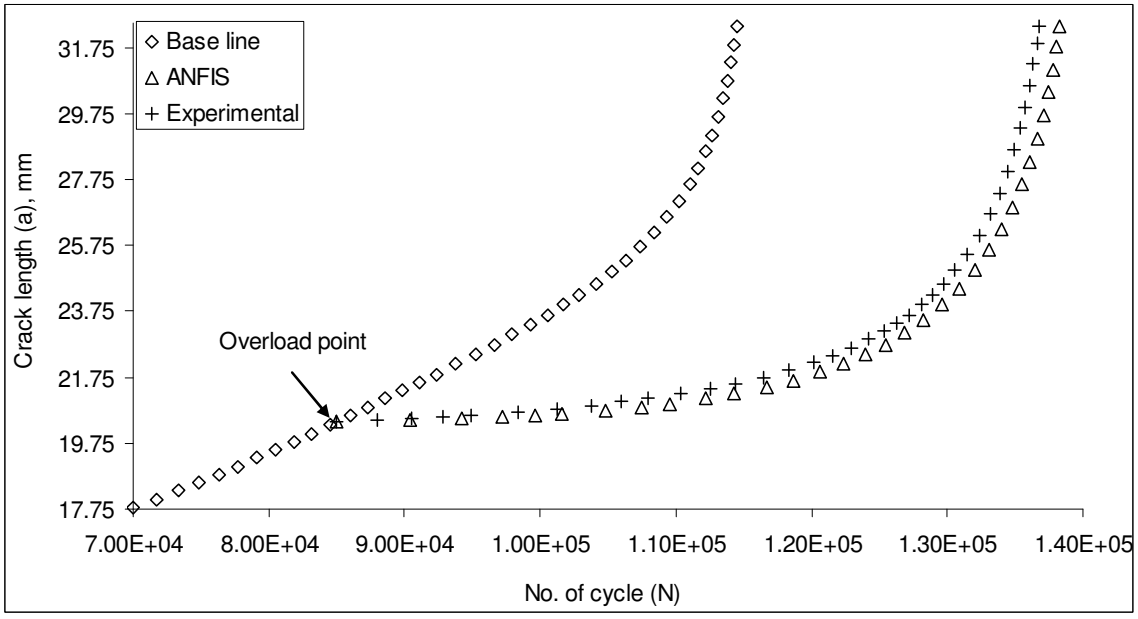

Fig. 12 – Comparison of predicted (ANFIS) and experimental crack length with number of cycle for Al 2024 T3

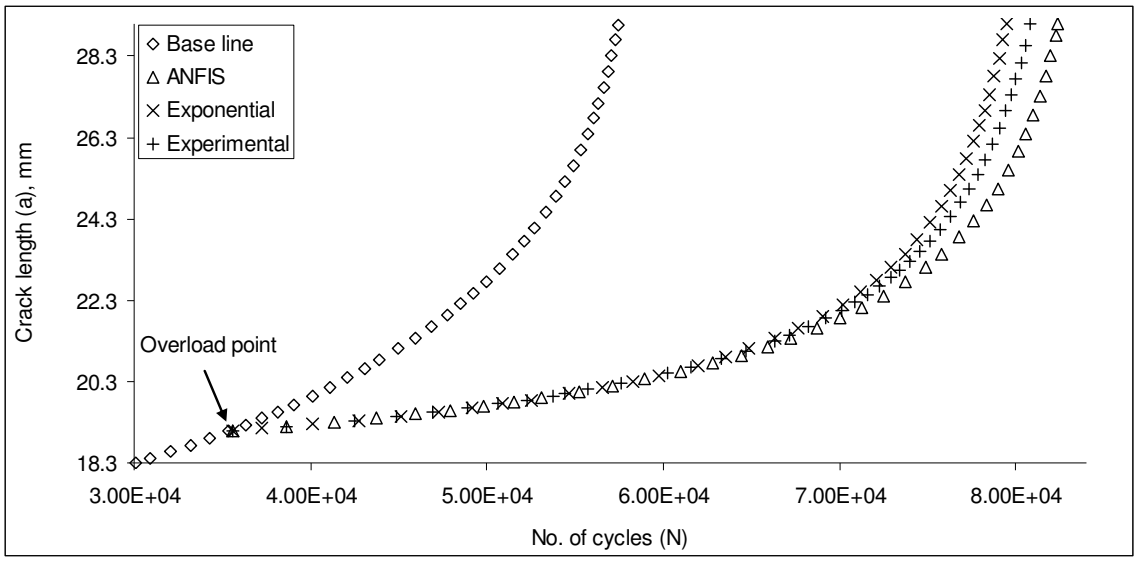

Fig. 13 – Comparison of predicted (ANFIS), exponential and experimental crack length with number of cycle Al 7020 T7

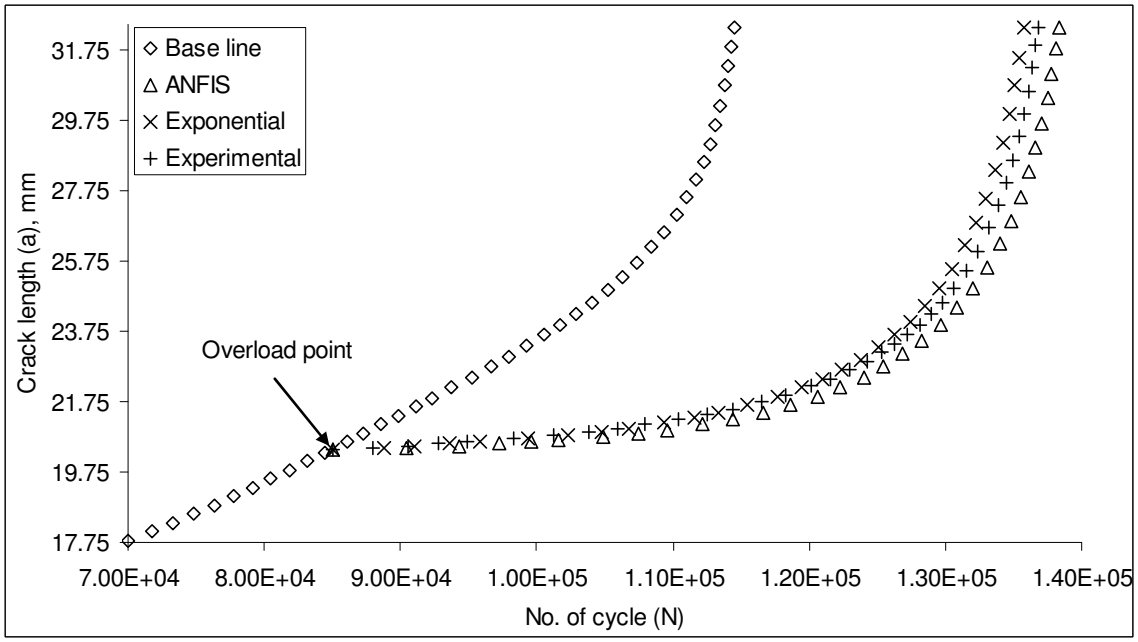

Fig. 14 – Comparison of predicted (ANFIS), exponential and experimental crack length with number of cycle Al 2024 T3

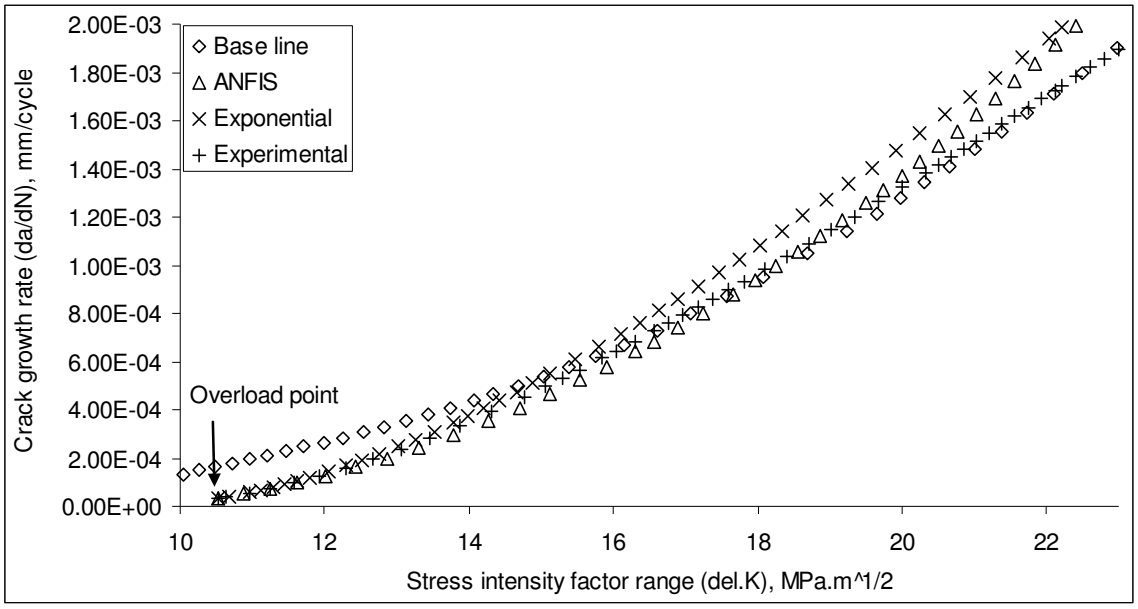

Fig. 15 – Comparison of predicted (ANFIS), exponential and experimental crack growth rate with stress intensity factor range for Al 7020 T7

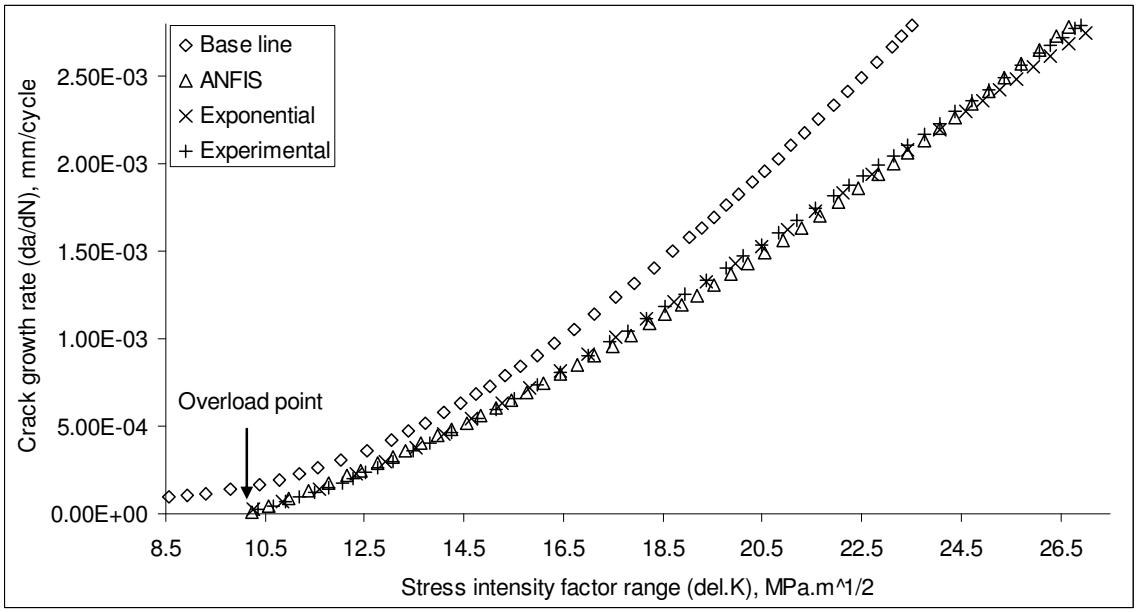

Fig. 16 – Comparison of predicted (ANFIS), exponential and experimental crack growth rate with stress intensity factor range for Al 2024 T3

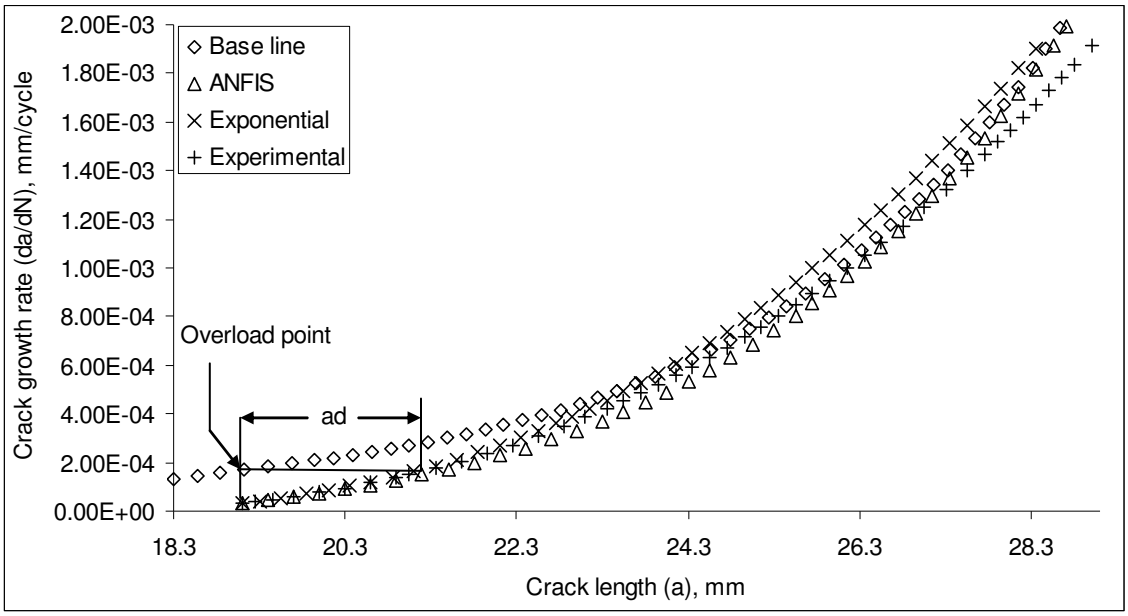

Fig. 17 – Comparison of predicted (ANFIS), exponential and experimental retarded crack length with stress intensity factor range for Al 7020 T7

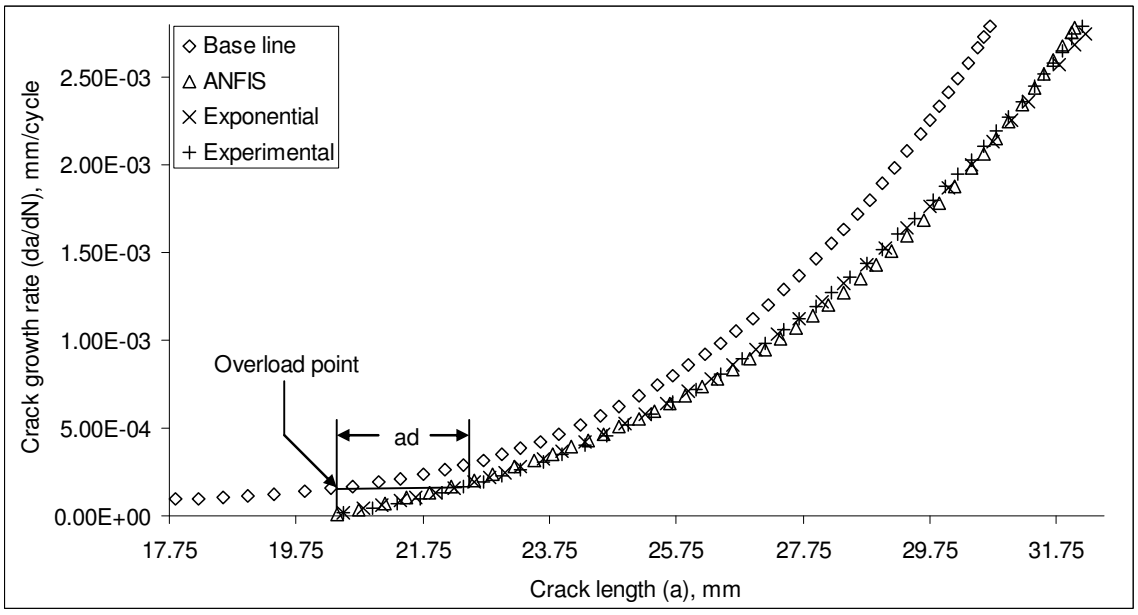

Fig. 18 – Comparison of predicted (ANFIS), exponential and experimental retarded crack length with stress intensity factor range for Al 2024 T3

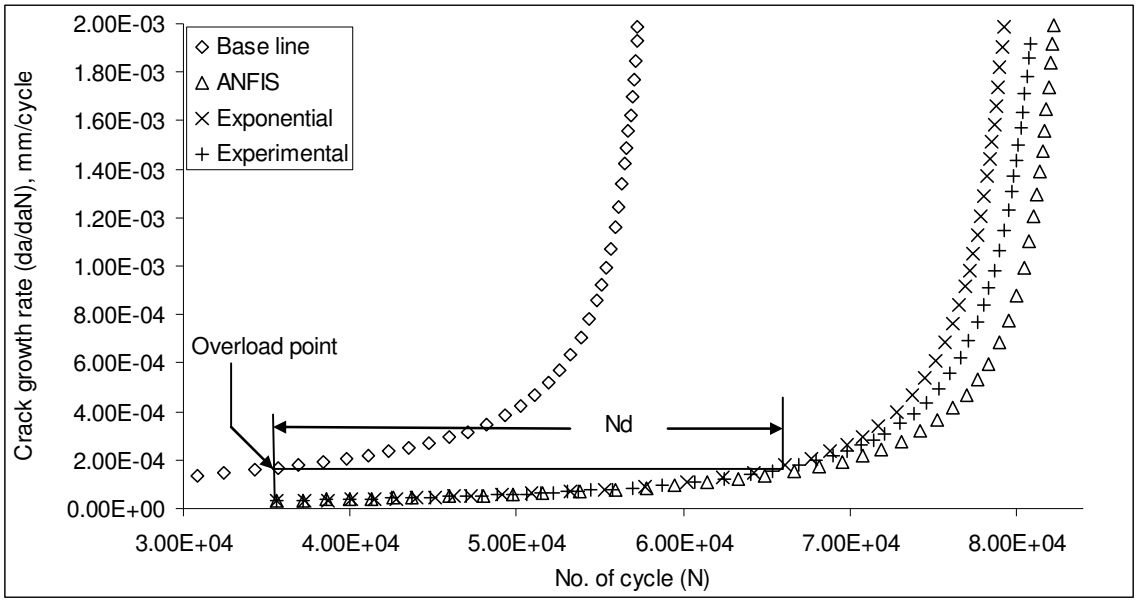

Fig. 19 – Comparison of predicted (ANFIS), exponential and experimental delay cycle with stress intensity factor range for Al 7020 T7

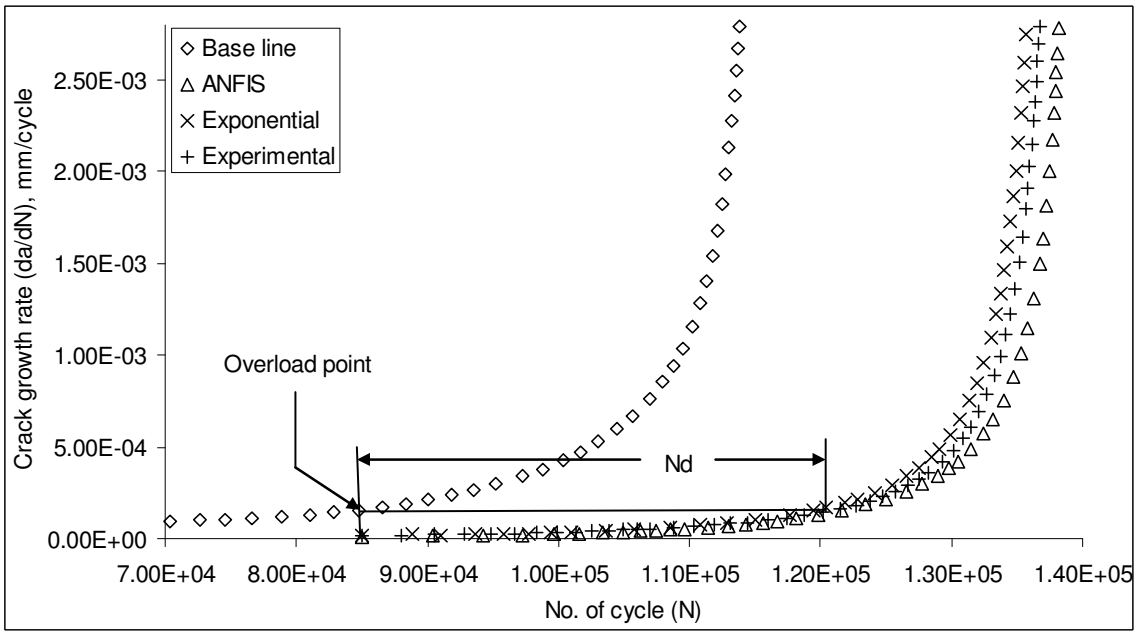

Fig. 20 – Comparison of predicted (ANFIS), exponential and experimental delay cycle with stress intensity factor range for Al 2024 T3

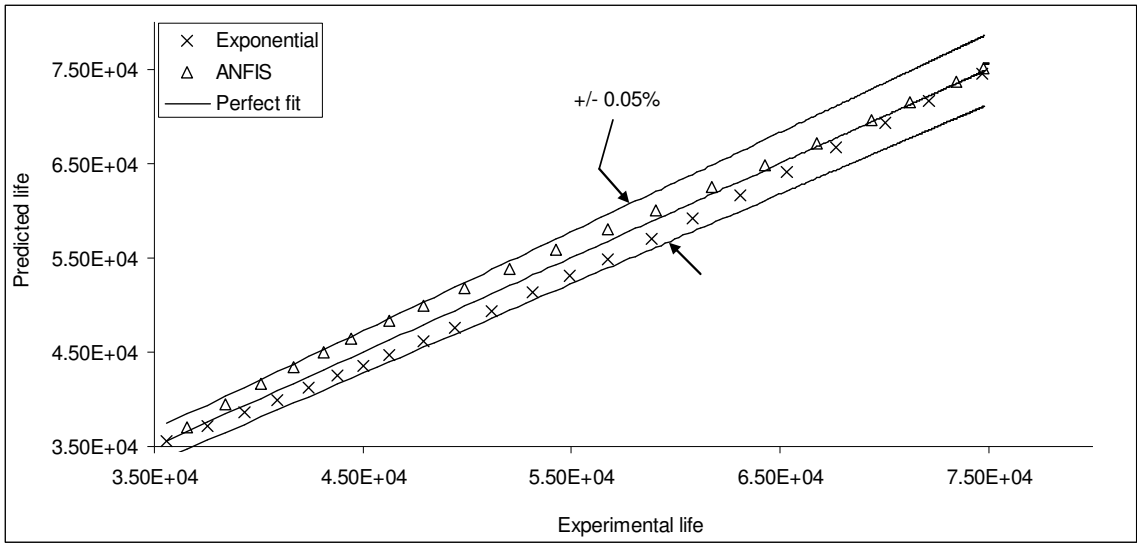

Fig. 21 – Error band scatter of predicted lives of 7020 T7 under mixed mode overload

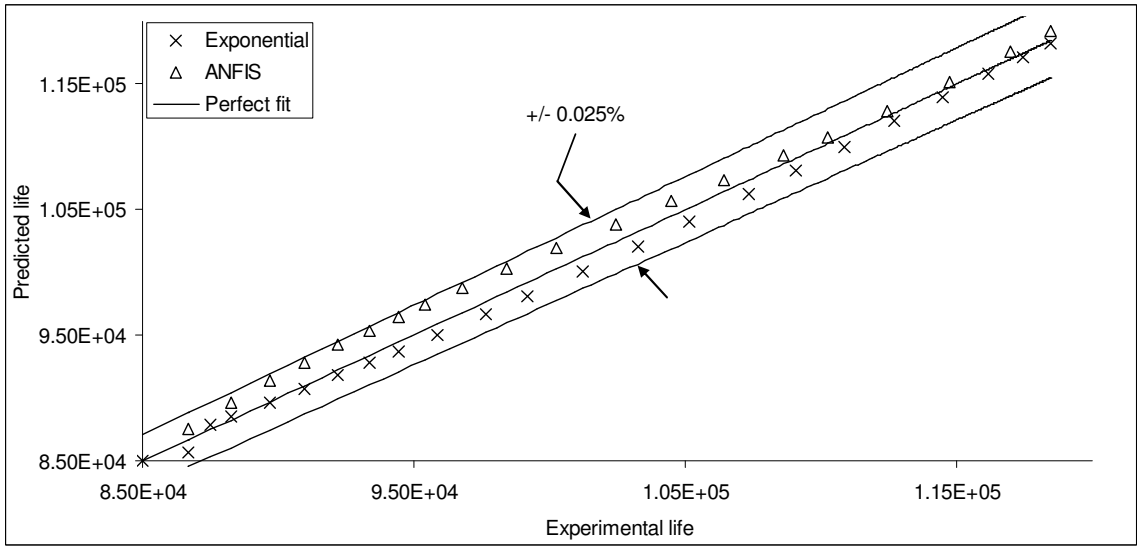

Fig. 22 – Error band scatter of predicted lives of 2024 T3 under mixed mode overload